American Mineralogist, Volume 105, pages 307–318, 2020

The distribution and abundance of halogens in eclogites: An in situ SIMS perspective of the Raspas Complex (Ecuador)

Benjamin M. Urann[1,2,*,†], Véronique Le Roux[2], Timm John[3], Grace M. Beaudoin[4], and Jaime D. Barnes[4]

[1]MIT-WHOI Joint Program, Marine Geology and Geophysics, Woods Hole Oceanographic Institution, Woods Hole, Massachusetts 02543, U.S.A.
[2]Geology and Geophysics Department, Woods Hole Oceanographic Institution, Woods Hole, Massachusetts 02543, U.S.A.
[3]Institut für Geologische Wissenschaften, Freie Universität Berlin, Malteserstrasse 74-100, 12249 Berlin, Germany
[4]Department of Geological Sciences, University of Texas, Austin, Texas 78712, U.S.A.

Abstract

We present in situ secondary ion mass spectrometry (SIMS) and electron microprobe analyses of coexisting garnet, omphacite, phengite, amphibole, and apatite, combined with pyrohydrolysis bulk-rock analyses to constrain the distribution, abundance, and behavior of halogens (F and Cl) in six MORB-like eclogites from the Raspas Complex (Southern Ecuador). In all cases concerning lattice-hosted halogens, F compatibility decreases from apatite (1.47–3.25 wt%), to amphibole (563–4727 μg/g), phengite (610–1822 μg/g), omphacite (6.5–54.1 μg/g), and garnet (1.7–8.9 μg/g). The relative compatibility of Cl in the assemblage is greatest for apatite (192–515 μg/g), followed by amphibole (0.64–82.7 μg/g), phengite (1.2–2.1 μg/g), omphacite (<0.05–1.0 μg/g), and garnet (<0.05 μg/g). Congruence between SIMS-reconstructed F bulk abundances and yield-corrected bulk pyrohydrolysis analyses indicates that F is primarily hosted within the crystal lattice of eclogitic minerals. However, SIMS-reconstructed Cl abundances are a factor of five lower, on average, than pyrohydrolysis-derived bulk concentrations. This discrepancy results from the contribution of fluid inclusions, which may host at least 80% of the bulk rock Cl. The combination of SIMS and pyrohydrolysis is highly complementary. Whereas SIMS is well suited to determine bulk F abundances, pyrohydrolysis better quantifies bulk Cl concentrations, which include the contribution of fluid inclusion-hosted Cl. Raspas eclogites contain 145–258 μg/g F and at least 7–11 μg/g Cl. We estimate that ~95% of F is retained in the slab through eclogitization and returned to the upper mantle during subduction, whereas at least 95% of subducted Cl is removed from the rock by the time the slab equilibrates at eclogite facies conditions. Our calculations provide further evidence for the fractionation of F from Cl during high-pressure metamorphism in subduction zones. Although the HIMU (high U/Pb) mantle source (dehydrated oceanic crust) is often associated with enrichments in Cl/K and F/Nd, Raspas eclogites show relatively low halogen ratios identical within uncertainty to depleted MORB mantle (DMM). Thus, the observed halogen enrichments in HIMU ocean island basalts require either further fractionation during mantle processing or recycling of a halogen-enriched carrier lithology such as serpentinite into the mantle.

Keywords: Eclogite, halogens, subduction, SIMS, nominally anhydrous minerals, HIMU; Halogens in Planetary Bodies

Introduction

Our understanding of the abundance and distribution of halogens in subducted slabs is limited. Hydrothermally altered oceanic crust (AOC) is thought to be a major halogen carrier during subduction, where F and Cl substitute into the hydroxyl sites of hydrous minerals such as amphibole and mica (Ito et al. 1983; Philippot et al. 1998; Van den Bleeken and Koga 2015; Barnes et al. 2018). Bulk estimates of pre-subduction AOC vary from 50–253 μg/g Cl and 216–400 μg/g F (Ito et al. 1983; Straub and Layne 2003; Barnes and Cisneros 2012; Van den Bleeken and Koga 2015; Chavrit et al. 2016). More recently, primary halogen measurements of altered oceanic crust from the East Pacific Rise (Penrose-type oceanic crust) and Atlantis Bank (SWIR, ultra-slow spreading) have shown extreme variability with both stratigraphic depth and lithology (Kendrick 2019a, 2019b). Bulk halogen measurements of blueschists and eclogites thought to represent high-pressure metamorphic AOC are also sparse. In a study of mélange rocks from Syros, Greece, Marschall et al. (2009) measured the bulk Cl content of eclogites (28–60 μg/g) and called into question previous estimates of eclogitized AOC Cl abundances, e.g., 100–200 μg/g Cl of Philippot et al. (1998), speculating that they may be overestimated. Pagé et al. (2016) analyzed a suite of blueschists from northwest Turkey; their results (8–22 μg/g Cl) also indicate that bulk eclogitized AOC could host less Cl than previously thought. Debret et al. (2016) reconstructed bulk halogen concentrations (57–79 μg/g Cl and 10–62 μg/g F) from in situ secondary ion mass spectrometry (SIMS) analyses for both blueschists and eclogites from the Western Alps, cautioning that typical bulk halogen measurements are

* E-mail: burann@whoi.edu. Orcid 0000-0001-5479-5070.
† Special collection papers can be found online at http://www.minsocam.org/MSA/AmMin/special-collections.html.

0003-004X/20/0003–307$05.00/DOI: https://doi.org/10.2138/am-2020-6994

not representative of prograde conditions due to potential retrogression during exhumation.

In situ halogen data in eclogitized AOC are also limited to a handful of studies, yet they provide important first-order observations. Debret et al. (2016) suggested that approximately 50% of F and 90% of Cl in the initial bulk-rock are lost to fluids during the first 80 km of subduction. Hughes et al. (2018) analyzed in situ halogen abundances of eclogites from the Western and Central Alps and provided eclogitized AOC estimates as low as 3 μg/g Cl. Finally, Pagé et al. (2016) reported low Cl and high F abundances in blueschist-hosted minerals and concluded that Cl is primarily expelled at shallow depths, whereas F is retained to at least 80 km depth.

Estimates of halogen fluxes in subduction zones are typically derived from the difference between the trench inputs and extrusive products of arc magmatism (e.g., Mather et al. 2006; Sadofsky et al. 2008; Pyle and Mather 2009; Freundt et al. 2014). Straub and Layne (2003) inferred a global arc recycling efficiency of 77–103% (Cl) and ~4–5% (F), implying near-total return of Cl to surface reservoirs, whereas most F is returned to the mantle. John et al. (2011) reached similar conclusions based on Cl mass balance constraints regarding in- and out-fluxes from the subducted slab perspective. Barnes et al. (2018) also concluded that F is efficiently returned to the mantle, however their estimated Cl fluxes are more variable, indicating that some Cl could be delivered back into the mantle by serpentinites (John et al. 2011; Kendrick et al. 2017). In a recent study, Pagé et al. (2018) found that Himalayan antigorite serpentinites host significant quantities of F (50–650 μg/g) and are enriched in Cl (8.8–35 μg/g) with respect to depleted mantle (11.0 μg/g F and 0.51 μg/g Cl; Salters and Stracke 2004). Taken together, these studies illustrate the challenge of estimating halogen input fluxes. A better understanding of the inherent variability within different lithologies used in flux calculations could help to refine such estimates.

In particular, the halogen content of eclogitized AOC remains largely unconstrained. Here we discuss the F and Cl abundances of Raspas Complex eclogites, a Cretaceous eclogite suite that we consider to be an ideal analog for subducted AOC. We combine in situ SIMS and EMP analyses of minerals with pyrohydrolysis-derived bulk halogen abundances and discuss the relative contribution of minerals, grain boundaries, and fluid inclusions to the total budget of halogens in subducted eclogites. Finally, we present new constraints on slab halogen fluxes and discuss the implications for the signature of eclogitized AOC in the HIMU mantle source.

Geologic context

An accreted parcel of oceanic lithosphere, the early Cretaceous Raspas Complex consists of blueschist- and eclogite-facies rocks (Feininger 1980, 1987; Maruyama et al. 1996). The high-pressure metamorphic suite is bound by the La Palma-El Guayabo Shear Zone to the north and lower grade greenschists and amphibolites to the south (Gabriele 2002). While no pillow structures or sheeted dikes were observed in the field, fluid-immobile REE and HFSE abundances, Nb/Zr and Hf/Yb systematics, TiO_2/Yb ratios, and Nd isotope systematics provide a well-reasoned rationale for inferred protoliths (John et al. 2010; Halama et al. 2011). Based on these characteristics, the blueschists and eclogites were derived from seamount-like basalt and normal mid-ocean ridge basalt (MORB) protoliths, respectively. Both underwent similar peak metamorphic conditions (based on major element thermobarometry) of ~600 °C to a maximum burial depth of approximately 60 km (John et al. 2010). Raspas eclogites show evidence for low-temperature seafloor alteration typical of basalts based on O isotopic compositions, and occur as two geochemically distinct groups: a MORB-type group (this study) with LREE depleted patterns, and a zoisite eclogite group characterized by significant incompatible trace-element enrichments that are interpreted to have been derived from serpentinite-derived dehydration fluids and that also display a fluid component indicative of some minor sediment contribution (Halama et al. 2011; Herms et al. 2012). Thus, the Raspas MORB-type group provides an excellent analog to study the in situ distribution of halogens in eclogitized AOC processed through subduction systems globally.

Sample description

We chose a set of six minimally retrogressed MORB-type eclogites that have been previously described by John et al. (2010). Samples consist of omphacite + garnet + rutile + apatite ± amphibole ± phengite ± quartz with minor secondary titanite. Subhedral to euhedral garnet porphyroblasts vary in size from <100 μm to 4 mm, often hosting inclusions of rutile and quartz. Some samples exhibit weakly deformed fabrics characterized by lineated omphacite. A single sample, SEC42-06, shows a strongly foliated texture with alternating layers of nearly monomineralic garnet and omphacite domains. Modal mineralogy varies significantly between samples, from nearly bimineralic garnet + omphacite to ~30% modal amphibole; such variability at similar *P-T* conditions is likely the result of bulk chemical compositional effects (Beinlich et al. 2010; John et al. 2010; Rebay et al. 2010). Representative photomicrographs of sample textures are presented in Figure 1 and Supplemental[1] Figure S1. Petrographic observations reveal near-ubiquitous fluid inclusions (FI). All samples contain variable quantities of FI hosted in omphacite and garnet, typically located in mineral cores (Fig. 1; see also Herms et al. 2012). In SEC46-02, monomineralic amphibole veinlets crosscut eclogite textures and contain secondary titanite overgrowths rimming rutile. Directly adjacent to these veinlets, FI-rich omphacite appears opaque in thin section (Fig. 1), which is unique to this sample and appears to reflect fluid infiltration.

Methods

SIMS

SIMS analyses were conducted at the Northeast National Ion Microprobe Facility (NENIMF) at the Woods Hole Oceanographic Institution using a Cameca IMS 1280. We follow the methods outlined in Urann et al. (2017), adding OH and S measurements to the protocol. 150 μm polished thick-sections were used for all analyses. Samples were cleaned with ethanol and deionized water to remove surface contamination, then placed in a vacuum oven to dry. Samples were gold-coated to ~160 nm thickness and placed into a vacuum chamber for storage until analysis. Samples were loaded into the instrument sample chamber at least 12 h prior to analysis, to allow adequate pump downtime and achieve chamber pressures of no more than $\sim 5 \times 10^{-9}$ torr. Each spot location was chosen to avoid surface cracks, which are known to influence analyses (Urann et al. 2017). A primary Cs^+ beam of 5.0–7.5 nA was sputtered through the sample surface with a 30×30 μm^2 raster and a 400 μm field aperture, allowing only transmission of ions from the

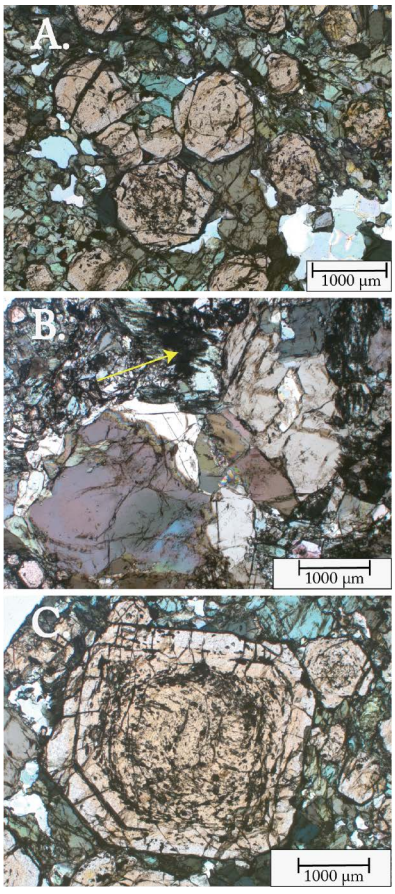

Figure 1. Representative photomicrographs of Raspas eclogite textures. (**a**) SEC43-03 contains garnet porphyroblasts within a matrix of omphacite and lesser quartz. (**b**) Amphibole veinlet in sample SEC46-02. Adjacent omphacite shows abundant fluid inclusions (yellow arrow). (**c**) SEC43-03 Megacrystic, inclusion-rich garnet showing sector zoning. (Color online.)

innermost 5 × 5 µm^2 of the beam crater. Secondary magnet mass calibration was done before each measurement with mass resolving power of >6000 (m/Δm at 10% peak height). We measured $^{19}F/^{30}Si$, $^{16}O^1H/^{30}Si$, $^{32}S/^{30}Si$, and $^{35}Cl/^{30}Si$ ratios in glass reference materials D51-3, D52-5, ALV519-4-1, 46D, 1649-3, 1654-3 6001, and AII107-D20 to produce a calibration slope for each one-week analytical session (Supplemental[1] Fig. S2). Calibration slopes (*m*) were obtained by plotting measured isotope ratios (*x*) against known reference material concentrations (*y*) of the form $y = mx$ for each element of interest. Sample unknowns were then calculated by multiplying measured ratios by *m*. Calibration slope uncertainties were assessed utilizing a bootstrapping technique (5000 iterations) to derive confidence intervals. Measurements where the internal precision (1 S.D.) was greater than 20% were screened and excluded from the data set; these low precision measurements (less than ten in total) were associated with elevated C (not reported) and Cl concentrations, and are likely the result of analyses conducted on micro-fractures. After screening, analytical uncertainties over five counting cycles (internal precision: typical standard error ~1% OH, <1.5% F, <3% Cl) were combined with calibration slope uncertainties (accuracy: typical uncertainty 6% OH, 5% F, <10% Cl, 95% confidence intervals) to yield no more than 8, 6, and 16% total uncertainty (2SE, 95% confidence intervals) for OH, F, and Cl measurements, respectively. Since mineral-specific calibrations are not well constrained and/or not available for halogens in most eclogitic phases, we used a basaltic glass calibration to present a unified data set that is self-consistent. This may introduce crystal-specific matrix effects, although preliminary calibrations of F in pyroxene and glass (Kumamoto et al. 2017) show slopes indistinguishable within uncertainty. Continuous measurements of ALV519-4-1 were used throughout the session to monitor instrument drift, which was found to be negligible. The OH, F, and Cl concentrations of Suprasil and Herasil 102, both optical-quality glasses, along with synthetic forsterite, were measured regularly in each session. There are no published values for the OH, F, and Cl content of Suprasil, Herasil 102 and synthetic forsterite, but those samples are believed to have very low OH, F, and Cl concentrations (less than 0.1 µg/g), respectively (E. Hauri, pers. comm.). To quantify our maximum backgrounds, we assume that Suprasil contains no OH, Herasil contains no F, and synthetic forsterite contains no Cl. Background OH, F, and Cl values were less than 7.3 µg/g, 0.19 µg/g, and 0.15 µg/g, respectively, for all sessions. Individual mineral analyses were not corrected for background when background values were less than propagated 2SE uncertainty; otherwise, measurements are corrected to remove backgrounds (Table 1). Cl measurement uncertainties on omphacite, garnet, and phengite are near parity with synthetic forsterite Cl values. We therefore subtracted our background Cl values from measured values for all bulk calculations.

EPMA

All mineral phases were analyzed using JEOL JXA-8200 electron microprobe (EMP) at the Massachusetts Institute of Technology. A 1 nA beam current and 15 kV accelerating potential were used for all analyses except apatite, which utilized a 10 nA beam current. Beam diameter was <1 µm for garnet and omphacite, and 10 µm for amphibole and phengite. Data reduction was done using CITZAF software (Armstrong 1995). The counting times used for phase analysis was 40 s on peak, and 20s on background. With respect to halogen abundances in amphibole and phengite, detection limits based on counting statistics were ~470 µg/g for F and ~60 µg/g for Cl. For apatite, care was taken to address known issues pertaining to fluorine excitation by electron microprobe analysis (Stormer and Pierson 1993). Peak searches were conducted only on the standard, and background was only measured on the first point for each grain. In addition, the LDE1 (W/Si) crystal was used for F measurements, which suppresses elemental interferences. Counting times for F were abbreviated to 10 s on peak and 40 s for P, Ca, and Cl while background counts were 5 s for F and 20 s for Ca, P, and Cl. Analytical uncertainties including background for F and Cl in apatite based on counting statistics were 3.4–4.4% and 7.2–11.6% (1σ), respectively, at concentrations of 1.47–3.25 wt% F and 192–515 µg/g Cl.

Bulk halogen measurements

Sample powders were washed in ultra-pure (18MΩ) deionized water and oven-dried overnight to avoid surficial Cl contamination by adsorption. This may have removed a portion of halogens along grain boundaries or in fluid inclusions; therefore we report Cl concentrations as minimums. We note that fluid inclusion dimensions (~1 to 10 µm, on average) are smaller than estimated powder grain size (<100 µm) and were likely retained, as demonstrated in a subsequent section. Halogens were extracted from approximately 2 g of sample powder by pyrohydrolysis in which a stream of water vapor captures volatiles as they are released from the sample during fusion by a gas torch. The vapor is condensed to produce an aqueous solution (Schnetger and Muramatsu 1996). From this solution, F and Cl concentrations are measured via ion chromatography (IC) using a Dionex Integrion HPIC System at the University of Texas at Austin. Detection limits of the analyzed solution are 0.05 µg/g for both F and Cl. The halogen content of the whole rock is then calculated using solution concentration, solution volume, and the mass of the powder melted. Using the JB-2 basalt reference material (98.5 µg/g F and 281 µg/g Cl; Imai et al. 1995), F and Cl yields are 75–83% and 68–95% (n = 5), respectively. Samples were analyzed with triple replicates in two batches. Since JB-2 yields are constrained within each contemporaneous batch, concentrations were yield-corrected by batch to the JB-2 reference material to more rigorously quantify absolute halogen concentrations. The yield correction assumes that standard yields and sample yields are similar. Although not perfect, this correction likely provides more accurate values. Both uncorrected and yield-corrected values are presented in this study for comparison. Reproducibility for each sample (precision) was combined with batch-specific JB-2 yield uncertainty (accuracy) to derive 1σ uncertainties. Replicate measurements of JB-2 and uncertainties are given in Supplemental[1] Table S9.

Modal mineralogy

We calculated the modal abundances of each phase by inverting the bulk-rock major element data of John et al. (2010) with EMP analyses of individual phases (Supplemental[1] Tables S1–S6). Although EMPA indicates zonation in some phases (e.g., TiO_2 and MnO), changes in modal proportions were negligible (often <1%

Table 1. Halogen abundances by phase (SIMS)

Sample	Description	No. grains analyzed	No. Analyses	F (µg/g)	F Error% (2SE Internal + Calibration Curve)	Cl (µg/g)	Cl background corrected (µg/g)	Cl Error % (2SE Internal + Calibration Curve)	OH (µg/g)	OH Error % (2SE Internal + Calibration Curve)	OH Error % (2SE Internal, Calibration, Background)	S (µg/g)
Clinopyroxene												
SEC42-06	Eclogite	1	1	50.6	6.0%	0.18	0.03	15.7%	651	5.5%		<0.1
SEC43-01	Eclogite	1	6	54.1	5.8%	0.13	0.00	14.6%	433	4.8%		<0.1
SEC43-03	Eclogite	1	3	16.7	4.5%	0.08	0.00	11.2%	773	5.8%		<0.1
SEC46-01	Eclogite	2	5	6.53	5.8%	0.11	0.03	10.5%	446	5.9%		<0.1
SEC46-02	Eclogite	1	3	13.4	6.0%	1.17	1.05	9.7%	753	7.7%		<0.1
SEC47-01	Eclogite	3	7	33.2	4.4%	0.07	0.00	12.4%	445	6.0%		<0.1
Garnet												
SEC42-06	Eclogite	2	5	8.92	6.0%	0.17	0.02	14.5%	113	5.1%	10.1	<0.1
SEC43-01	Eclogite	2	9	7.76	6.0%	0.18	0.03	14.0%	125	5.2%	10.8	<0.1
SEC43-03	Eclogite	2	6	2.01	6.1%	0.10	0.02	11.5%	201	5.7%	18.8	<0.1
SEC46-01	Eclogite	2	7	1.73	5.1%	0.11	0.03	10.0%	85	5.9%	12.3	<0.1
SEC46-02	Eclogite	2	6	4.76	6.1%	0.11	0.00	11.8%	60	7.6%	13.8	<0.1
SEC47-01	Eclogite	3	3	3.81	5.3%	0.08	0.00	11.7%	80	6.2%	12.2	<0.1
Phengite												
SEC42-06	Eclogite	1	2	610	5.9%	2.13	1.98	12.7%	22452	4.6%		0.65
SEC43-01	Eclogite	1	9	1822	5.9%	1.16	1.01	12.6%	28360	4.6%		0.54
SEC43-03	Eclogite											
SEC46-01	Eclogite											
SEC46-02	Eclogite											
SEC47-01	Eclogite	2	6	645	4.4%	1.22	1.14	8.7%	26410	5.7%		0.48
Amphibole												
SEC42-06	Eclogite	1	5	1812	4.7%	82.7	82.6	13.1%	18682	4.2%		27.9
SEC43-01	Eclogite	1	3	4727	5.9%	11.6	11.5	12.2%	20187	4.6%		18.0
SEC43-03	Eclogite	1	2	1073	4.6%	0.64	0.56	8.5%	17952	5.9%		27.0
SEC46-01	Eclogite	4	8	747	5.5%	10.3	10.3	8.7%	17292	5.9%		5.6
SEC46-02	Eclogite	2	6	563	6.2%	11.8	11.7	8.6%	23449	7.5%		5.9
SEC47-01	Eclogite	1	3	1127	5.0%	15.5	15.4	8.6%	15747	5.8%		3.0
Titanite												
SEC46-02	Eclogite	1	3	1394	6.0%	0.11		9.7%	4010	7.4%		<0.1

(Table extends on next page)

difference) when varying mineral compositions were used. We performed our calculations by taking the mean composition for each phase. SiO_2, TiO_2, Al_2O_3, FeO, MnO, MgO, CaO, Na_2O, K_2O, and P_2O_5 were used in the minimization. P_2O_5 was assumed to reside entirely within apatite. Calculated modes agree well with independently estimated mineral modes based on optical microscopy. Calculated mineral modes and uncertainties are shown in Table 2.

All eclogite samples contain >35 modal percent of garnet. Omphacite modal proportions range from 23–53 vol%, whereas phengite, when present, makes up 2–4 vol% of the bulk-rock modally. Samples contain varying modal proportions of amphibole, from 0.5 to ~30 vol%. Quartz, when present, is up to 8 vol% of the bulk rock whereas rutile (1–2 vol%) and apatite (0.25–1.6 vol%) are omnipresent.

Results

Major element variability by EMPA

Major element profiles show garnet zonation with respect to end-member components almandine, pyrope, grossular, and spessartine (Supplemental[1] Table S1). Garnet porphyroblast cores are often elevated in the spessartine component as well as TiO_2, with a gradual decrease toward the rim consistent with prograde garnet growth.

Omphacite (Cpx) Mg# [molar Mg/(Mg+Fe)] varies from 0.68 to 0.79 (Supplemental[1] Table S2) and correlates negatively with Cpx abundances, reflecting the influence of bulk-rock chemistry on mineral modes. Omphacite EMPA profiles show some intra-mineral zonation; in particular, SEC42-06 and SEC43-01 show increasing Si concentrations from the core to rim, while SEC43-03 Si content decreases from core to rim. Mg# remain uniform within single grains.

Phengite was analyzed in samples SEC42-06, SEC43-01, and SEC47-01 (Supplemental[1] Table S5). SEC42-06 is relatively homogeneous, with slight Na enrichment approaching the rim. A full rim-to-rim profile in SEC43-01 shows strong zonation with increases in Na and Al from core to rim, and decreases in Si, K, Fe, and Mg (Supplemental[1] Fig. S3). SEC47-01 shows slight Si, K, and Mg rim depletions. Both phengite profiles are consistent with continued grain growth or partial recrystallization during decompression due to decreasing Si from core to rim (Massonne and Schreyer 1987).

Table 2. Calculated mineral modes

	Phase fraction									
Est. Modal Abundances	Garnet	Omphacite	Phengite	Amphibole	Quartz	Rutile	Titanite	Apatite	SUM	NAMs (Grt+Cpx+Qtz)
SEC 42-06	0.421(32)	0.534(32)	0.015(2)	0.0050(5)	0	0.021(2)	0	0.0040(4)	1	0.96
SEC 43-01	0.384(30)	0.524(31)	0.045(4)	0.010(1)	0.017(2)	0.018(2)	0	0.0030(3)	1	0.92
SEC 43-03	0.378(28)	0.416(28)	0	0.099(10)	0.087(2)	0.016(2)	0	0.0040(4)	1	0.88
SEC46-01	0.456(28)	0.229(21)	0	0.297(25)	0	0.016(2)	0	0.0025(3)	1	0.68
SEC46-02	0.358(27)	0.346(27)	0	0.248(22)	0	0.010(1)	0.02(1)	0.016(2)	1	0.70
SEC47-01	0.406(31)	0.499(31)	0.044(4)	0.0050(5)	0.024	0.018(2)	0	0.0040(4)	1	0.93
Average mineral modes	0.41	0.43	0.011	0.107	0.023	0.000	0.018	0.006	1.000	

Note: Values in parentheses represent 1σ uncertainty

TABLE 1.—*EXTENDED*

Sample	S Error % (2SE Internal+ Calibration Curve)	Intra-sample Variability F, 1σ	OH, 1σ	Cl, 1σ
	Clinopyroxene			
SEC42-06	12.6%	–	–	–
SEC43-01	15.5%	15%	13%	–
SEC43-03	9.2%	3%	3%	–
SEC46-01	8.4%	4%	5%	–
SEC46-02	9.2%	5%	10%	25%
SEC47-01	13.4%	24%	14%	–
	Garnet			
SEC42-06	11.4%	24%	16%	–
SEC43-01	16.1%	29%	67%	–
SEC43-03	9.2%	42%	10%	–
SEC46-01	11.5%	93%	27%	–
SEC46-02	10.5%	35%	22%	–
SEC47-01	10.4%	12%	7%	–
	Phengite			
SEC42-06	8.4%	6%	1%	4%
SEC43-01	7.6%	8%	4%	20%
SEC43-03				
SEC46-01				
SEC46-02				
SEC47-01	5.7%	7%	9%	9%
	Amphibole			
SEC42-06	11.0%	18%	5%	37%
SEC43-01	5.9%	3%	3%	24%
SEC43-03	4.4%			
SEC46-01	5.3%			
SEC46-02	6.1%			
SEC47-01	5.2%			
	Titanite			
SEC46-02				

Amphibole occurs as several different species that likely reflect bulk compositional variations; analyses are presented in Supplemental[1] Table S4, along with IMA 2012 recommended nomenclature calculated using the routine of Locock (2014). SEC42-06, SEC43-01, and SEC43-03 are Na-Ca subgroup katophorite, SEC46-01 and SEC46-02 are Ca subgroup pargasite, and SEC47-01 is classified as a Na-Ca subgroup winchite. Nearly all EMP analyses show Cl abundances at or below the detection limit of ~60 µg/g. However, F concentrations show significant intra-grain variability, differing by as much as a factor of two from core to rim (e.g., SEC42-06, 869–1834 µg/g).

Apatite halogen contents range from 1.47–3.25% wt% F and 0.019–0.051 wt% Cl (Supplemental[1] Table S5). The hydroxyl content of the apatite is taken as the oxide sum subtracted from one hundred, which classifies apatite in samples SEC43-03, SEC46-01, SEC46-02, and SEC47-01 as hydroxylapatite and apatite in sample SEC43-01 and SEC42-06 as fluoroapatite. Apatite halogen abundances are similar to apatite from other blueschist and eclogite metamorphic terranes with low Cl abundances (Pagé et al. 2016; Hughes et al. 2018) whereas some HP terranes developed from oceanic protoliths also contain Cl-rich apatite (John and Schenk 2003). Typical MORB (0.164 wt% P_2O_5, Gale et al. 2013) must undergo significant fractional crystallization (>70%) before reaching apatite saturation (~0.7 wt% P_2O_5); indeed, apatite-saturated MORB are few (Anderson and Greenland 1969; Watson 1979). Based on the bulk rock chemistry of Raspas provided by John et al. (2010) these conditions are unlikely to have been met. Therefore interstitial grains most likely formed as new growth during progressive metamorphism.

Halogen and water variability

Bulk-rock pyrohydrolysis analyses are presented in Table 3. As noted previously, we report both yield-corrected and uncorrected halogen abundances. Yield-corrected F and Cl concentrations for all samples were 115–199 µg/g and 6.7–19.9 µg/g, respectively. In situ halogen measurements are presented in Tables 1 and Supplemental[1] Table S5. Resolvable intra- and inter-grain heterogeneity is observed for F and OH in all phases both in single-grain SIMS profiles (Supplemental[1] Table S7) and in multiple grains from the same sample.

Halogen variability is notable in nominally anhydrous minerals (NAMs), particularly garnet with both inter- and intra-grain heterogeneity observed (Table 1, Supplemental[1] Fig. S4, and Supplemental[1] Table S7). Grain-averaged sample values range from 1.7–8.9 µg/g F and 60–201 µg/g OH, while Cl is always at or near detection limits. Intra-sample garnet F and OH variability are up to 93% and 67%, respectively (1σ, Table 1). Variations from core to rim were not systematic, nor can they be attributed to analytical uncertainty; in some cases cores were enriched in F or OH relative to rims, while in other grains the case was reversed. Core and rim measurements for OH and F are presented in Figure 2, illustrating that while some intragrain variability is

TABLE 3. Halogen bulk rock abundances, ratios

	Calculated bulk (WHOI)			Uncorrected for yield Pyrohydrolysis		Corrected for yield Pyrohydrolysis (UTA)		Uncertainty (yield corrected) 1 SD propogated (UTA)		Calculated/ measured bulk				
Sample	OH µg/g	F µg/g	Cl µg/g	F µg/g	Cl µg/g	F µg/g	Cl µg/g	F (µg/g)	Cl (µg/g)	F %	Cl %	Cl/Nb[b]	Cl/K[b]	F/Nd[b]
SEC42-06	901	168	2.5	92	8.9	115	11.0	15	2.2	146%	23%	3.03	0.0089	10.8
SEC43-01	1783	258	1.4	109	7.1	137	8.9	68	3.1	189%	16%	4.34	0.0020	22.5
SEC43-03	2342	200	0.8	152	5.4	189	6.7	11	2.2	105%	12%	2.80	0.0116	15.8
SEC46-01	5123	241	3.2	154	9.1	193	11.3	52	3.1	125%	28%	5.18	0.0085	17.3
SEC46-02	6836	415	8.2	160	16.1	199	19.9	12	2.4	208%	41%	4.68	0.0218	32.1
SEC47-01	1663	145	1.3	112	7.1	139	8.8	9.1	1.5	104%	15%	4.23	0.0021	11.2
Average		237.7	2.9	129.8	8.9	162.0	11.1							
Standard deviation		96.6	2.7	29.2	3.8	36.1	4.6							
Average[a]		202.3	1.85	123.7	7.5	154.5	9.4					3.9	0.0066	15.5
Standard deviation[a]		47.7	0.99	28.0	1.51	34.9	1.88					1.0	0.0043	4.8
AOC (Barnes et al. 2018)		216	207											
Average reycling efficiency (to mantle)		93.7%	0.9%	57.3%	3.6%	71.5%	4.5%							

[a] Excludes SEC46-02 due to retrograde alteration. Values used in bulk flux calculations.
[b] Cl and F values from yield corrected pyrohydrolysis, K, Nb, Nd using bulk-rock chemistry from John et al. (2010).

present, most grains plot on or near 1:1 lines within uncertainty.

Omphacite has highly variable F abundances (6.5–54.1 µg/g) while OH range from 445 to 773 µg/g. Similar to garnet, Cl abundances are less than 0.1 µg/g for five of the six samples. However, SEC46-02 yields significantly higher mean Cl abundances of 1.05 µg/g. F and OH variability within a single sample was less than 24% and 14%, respectively. A profile of Cpx from SEC43-01 exemplifies core to rim variations, with F and OH concentrations of 42.1–69.7 µg/g and 362–557 µg/g, respectively (Supplemental[1] Fig. S5). While these variations are discernable, heterogeneity in this grain is 15% or less for all three species; core to rim variations are modest and typically plot along a 1:1 line, within uncertainty (Fig. 2).

Amphibole occurs as both interstitial grains and monomineralic veinlets, with veins only occurring in SEC46-02. Interstitial amphibole yields F and Cl abundances of 747–4727 µg/g and 0.56–82.6 µg/g, respectively. Pargasite veins from SEC46-02 contain on average 563 µg/g F and 11.7 µg/g Cl. Single sample averaging produces variability of no more than 18% for F and 37% for Cl (1σ).

Phengite from three samples contains 610–1822 µg/g F and 1.01–1.98 µg/g Cl. Two of the three grains analyzed show no systematic core to rim halogen variations. Phengite is relatively homogeneous in terms of F and Cl, with 1σ sample variations of less than 20%. However, in a rim to rim transect of SEC43-01 phengite (Supplemental[1] Fig. S6), intra-grain variability is evident. F concentrations show a systematic decrease from core to rim, paralleling major element trends of decreasing K_2O, SiO_2, and MgO. Cl is enriched near grain boundaries by approximately 40% with respect to cores, following Al_2O_3 and Na_2O rim enrichments (Supplemental[1] Figs. S3 and S6). Finally, a single secondary titanite in SEC46-02 contains 1394 µg/g F, <0.1 µg/g Cl, and 4010 µg/g OH.

Discussion

Halogen redistribution during eclogitization

Halogen distribution during prograde metamorphism depends to a large extent on bulk-rock chemistry, which dictates the equilibrium mineral assemblage and phase proportions at any given pressure and temperature. Raspas eclogites show a strong positive correlation between the proportion of omphacite in the bulk-rock and the F content of omphacite (Supplemental[1] Fig. S7), suggesting that F is repartitioned during eclogitization and progressive omphacite growth. In addition, we compare the modal proportion of nominally anhydrous minerals (omphacite + garnet + quartz) to the volatile content of analyzed phases (Supplemental[1] Fig. S8). As the proportion of NAMs in the bulk assemblage increases, the F content of each phase shows a commensurate increase. Indeed, modal abundances of amphibole are negatively correlated with F concentrations in both omphacite and apatite, again suggesting effective redistribution of F during prograde metamorphism. Further, apatite Cl abundances increase as amphibole modes decrease and the mineral assem-

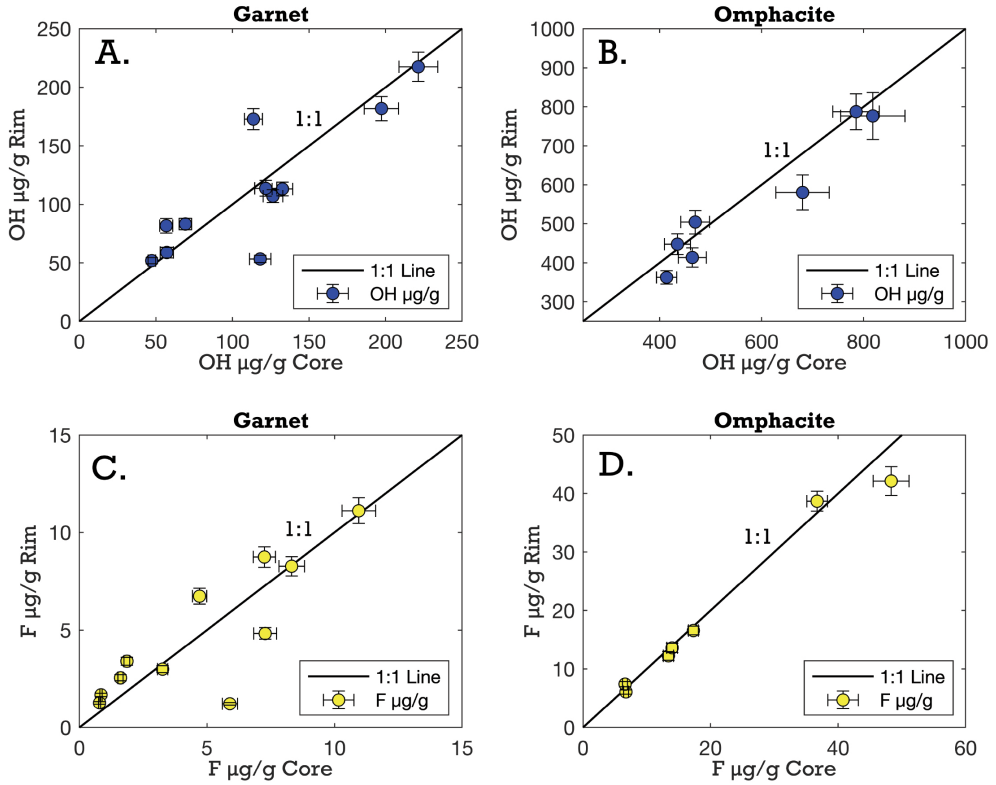

Figure 2. Core and rim measurements for OH (**a** and **b**) and F (**c** and **d**) in garnet and omphacite. The majority of samples show core and rim values that fall on a 1:1 line, within uncertainty, allowing a high degree of confidence in bulk-rock calculations based on in situ measurements. Error bars are 2SE. (Color online.)

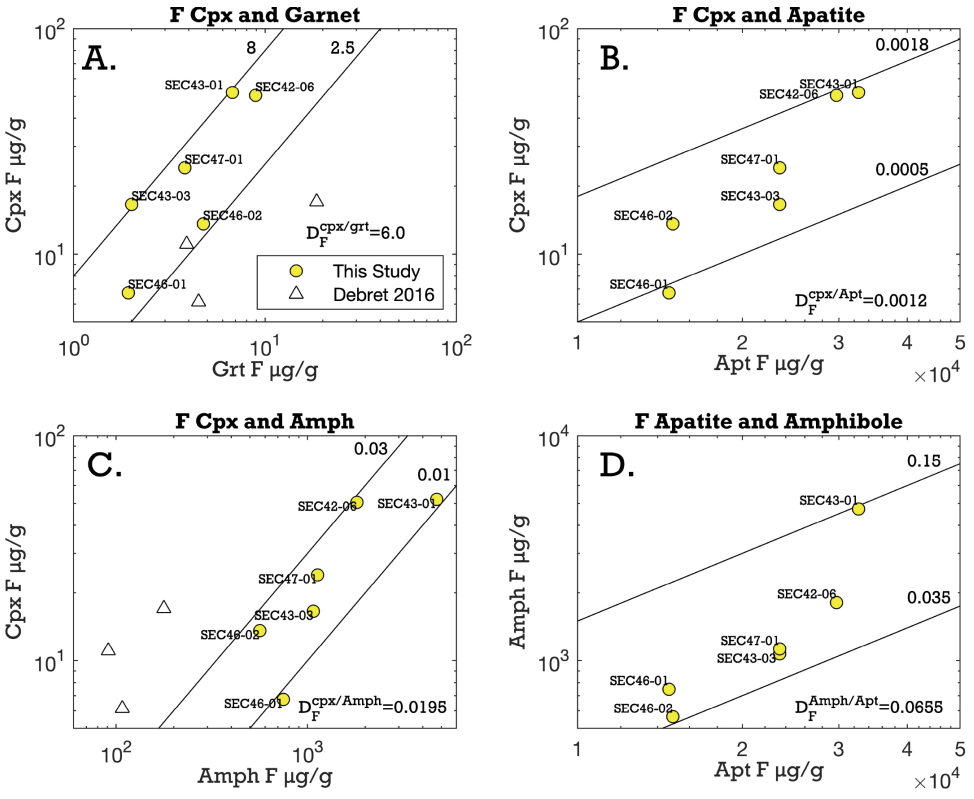

Figure 3. Inter-mineral F partitioning between (**a**) omphacite and garnet, (**b**) omphacite and apatite, (**c**) omphacite and amphibole, and (**d**) omphacite and phengite. White triangles are literature data from Debret et al. (2016). Solid lines show constant inter-mineral partition coefficients (labeled), while mean partition coefficients for each mineral pair are presented in the bottom right panel corner. (Color online.)

blage becomes dominated by garnet and omphacite. In all cases concerning lattice-hosted halogens, F is accommodated primarily in apatite (1.47–3.25 wt%), amphibole (563–4727 µg/g), and phengite (610–1822 µg/g) with lesser amounts in omphacite (6.5–54.1 µg/g) and garnet (1.7–8.9 µg/g). In addition, Cl is primarily hosted in apatite (192–515 µg/g), with lesser amounts in amphibole (0.64–82.7 µg/g), phengite (1.2–2.1 µg/g), omphacite (<0.05–1 µg/g), and garnet (<0.05 µg/g).

Our in situ measurements permit the calculation of distribution coefficients between various phases of interest (Figs. 3 and 4, Supplemental[1] Table S8). Given the scarcity of data, these new values provide important constraints on the distribution of F and Cl in eclogitic phases. Several observations can made from the above distribution coefficients. First, F partitioning between mineral pairs defines a narrow range and appears to be insensitive to concentrations, which in some cases span nearly an order of magnitude. Second, as expected, apatite will preferentially host crystal lattice-bound F and Cl when present in eclogitic assemblages, similar to apatite's halogen affinity in the presence of aqueous fluids (Kusebauch et al. 2015). Finally, F and Cl are preferentially partitioned into amphibole over phengite in all samples by a factor of 2.4 and 20, respectively. Interestingly, this observation is in contrast to blueschists studied by Pagé et al. (2016) who found $D_F^{Amph\text{-}Phen}$ was always less than unity, whereas $D_{Cl}^{Amph\text{-}Phen}$ was approximately equal to one within error. Hence, blueschist to eclogite phase transformations may elicit changes in the relative compatibilities of halogens between coexisting phases, likely as a function of changing modal proportions, mineral compositions (e.g., glaucophane to katophorite), and *P-T* conditions.

Comparison between measured and reconstructed bulk halogen abundances

Using mineral modes, in situ SIMS data, and EPMA halogen concentrations, we calculate a reconstructed bulk-rock F and Cl content for each eclogite sample, which can then be compared to bulk values measured by pyrohydrolysis (Table 3, Fig. 5). Both raw (not corrected for yield) and yield-corrected pyrohydrolysis halogen abundances are given in Table 3. We use yield-corrected concentrations in subsequent discussions.

Reconstructed concentrations and pyrohydrolysis measurements yield F concentrations of 168–415 µg/g and 115–199 µg/g, respectively. Reconstructed F abundances are broadly concordant with measured values; three of the six samples agree within uncertainty, whereas three samples display higher reconstructed values (Fig. 6; Table 3). The relative congruence between reconstructed and measured F values implies that F may be entirely hosted within the crystal lattice of eclogitic phase assemblages. The discrepancy observed for three of the six samples may be due to a combination of factors including uncertainties in pyrohydrolysis yields (Supplemental[1] Table S9) that are typically larger than SIMS analyses, inter-grain halogen heterogeneity, or uncertainties in the calculated modal proportions (Table 2). We

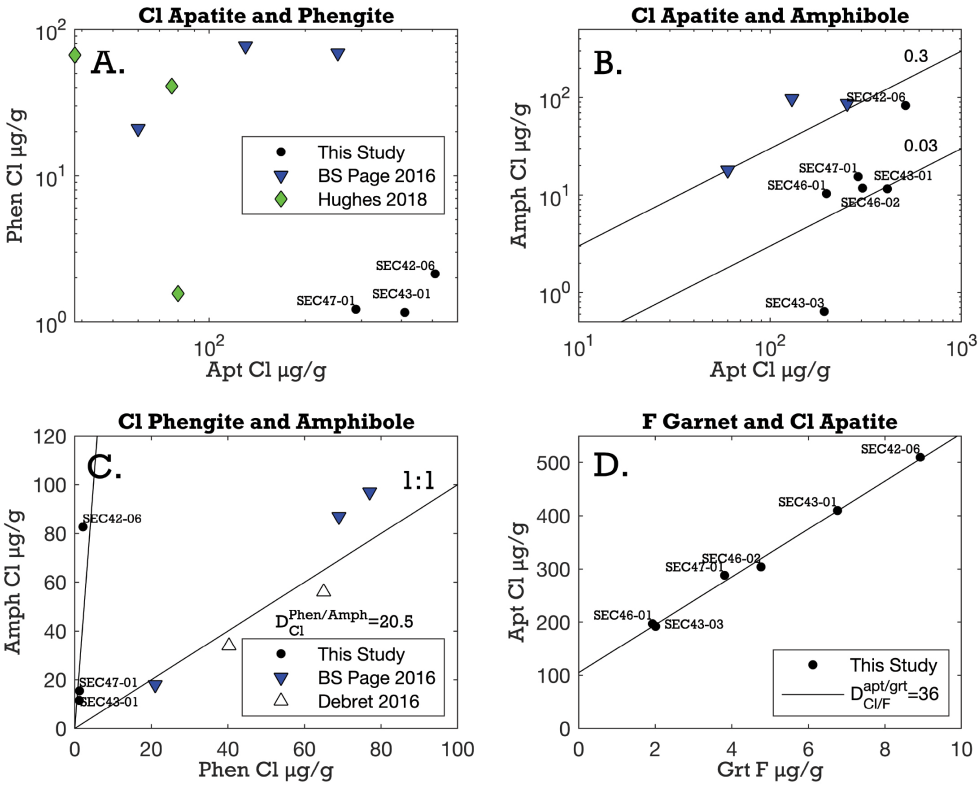

Figure 4. Inter-mineral Cl partitioning between (**a**) phengite and apatite, (**b**) apatite and amphibole, (**c**) phengite and amphibole, and (**d**) apatite Cl and garnet F concentrations. White triangles are literature data from Debret et al. (2016), green diamonds from Hughes et al. (2018) and blue upside down triangles from Pagé et al. (2016). Solid lines denote constant inter-mineral partition coefficients as in Figure 3. (Color online.)

note that calculated modal proportions as derived from whole rock analysis were assessed, but found to be minor.

Bulk reconstructed and measured Cl concentrations for all samples are 0.8–8.2 µg/g and 6.7–19.9 µg/g, respectively. Unlike F, Cl shows very large and systematic discrepancies between reconstructed and measured values, with reconstructed values representing only 12–41% of the pyrohydrolysis-derived bulk values. We discuss these drastic differences below, in terms of uncertainties and possible means of reconciliation between the two methods. We consider three possible processes to explain the difference: retrograde alteration, grain boundary hosted Cl and Cl-bearing fluid inclusions.

Bulk halogen analyses rely on the assumption that samples are perfectly preserved and have not been retrogressed along their exhumation path. Even minute amounts of alteration (e.g., chlorite or titanite) can drastically affect such bulk measurements (Debret et al. 2016). Most Raspas eclogites appear to be pristine with little to no visible alteration or retrogression, with the exception of SEC46-02 that contains titanite-on-rutile overgrowths and monomineralic amphibole veinlets adjacent to FI-rich omphacite, indicating possible fluid assimilation. This sample also displays elevated reconstructed (8.2 µg/g) and bulk (19.9 µg/g) Cl compared to the rest of the suite. In light of this suspected fluid assimilation, and the large F incongruity (~100%) between the two methods, we exclude this sample from subsequent bulk rock calculations. Minor retrogression may have contributed to the discrepancy for SEC46-02, however all other samples still show at least a factor of three difference between reconstructed and measured bulk Cl concentrations. Therefore, a factor other than late alteration is likely at play.

To further explore this discrepancy, we conducted additional SIMS analyses on grain boundaries of FI-free amphibole and garnet (Supplemental[1] Fig. S9). Both profiles across grain boundaries display pronounced spikes in $^{35}Cl/^{30}Si$ signals within the immediate grain boundary at near-constant ^{30}Si counts. These grain boundary measurements are equivalent to 7–18 µg/g Cl. Yet, the grain boundaries themselves are far smaller than the dimensions of our analysis spot (3.8 × 3.8 µm) and, depending on their size, could contain >1 wt% Cl assuming a grain boundary thickness of 5 nm or less. As grain boundary porosity values in eclogites are poorly constrained, we used Equation 9.6 of Turcotte and Schubert (2002) to calculate grain boundary porosity values based on a simplified grain geometry over a range of grain boundary thicknesses (1–25 nm) with realistic grain sizes (500 µm) to yield values of 9×10^{-12} to 6×10^{-9} (Supplemental[1] Table S10). The Cl contribution from grain boundaries alone (<0.1 µg/g Cl in all cases, or <2% contribution compared to pyrohydrolysis Cl abundances), given the above parameters, is unable to reconcile the reconstructed vs. measured Cl abundances.

Finally, we consider the possible role of fluid inclusions, as they could represent an important host for Cl (Philippot and Selverstone 1991; Herms et al. 2012; Kendrick 2018). FI (~1 to 10 µm on average) are found ubiquitously hosted in garnet (Supplemental[1]

Fig. S1C) and omphacite cores, both of which appear in textural equilibrium with adjacent phases and occur in all samples. FI are far more abundant in SEC46-02, in particular where omphacite is in contact with monomineralic pargasitic amphibole veinlets (Fig. 1b). FI appear cloudy in thin section owing to their prolific abundance. These features likely reflect crystallization in the presence of fluids, possibly during prograde conditions (e.g., John et al. 2010; Herms et al. 2012); such features have also been noted elsewhere in previous studies (e.g., Zack et al. 2001; Massonne 2012). Although we cannot directly analyze fluid inclusions by SIMS, heterogeneous Cl enrichments in SEC46-02 FI-rich omphacite (44–94 µg/g Cl) indicate that each SIMS analysis may incorporate some Cl-rich FI material. FI-free (optically clear) omphacite from the same sample also contains an order of magnitude more Cl (1.05 µg/g) compared to omphacite from all other samples (<0.1 µg/g), which is consistent with assimilation of pervasive fluids during crystallization (Herms et al. 2012). FI may host significant quantities of Cl from hundreds of µg/g to >10 wt% NaCl equivalent (Philippot and Selverstone 1991; Philippot et al. 1998; Scambelluri and Philippot 2001; Svensen et al. 2001; Kendrick et al. 2015; Kendrick 2018). Herms et al. (2012) have shown that omphacite and garnet hosted FIs from Raspas contain ~2 wt% NaCl, congruent with the salinity of dehydration-related FI found in rocks that have undergone blueschist-to-eclogite conversion (Gao and Klemd 2001). Assuming that FI contain ~2 wt% NaCl and represent 0.05–0.1% of the total sample volume, one may reconcile the discrepancy between in situ and bulk Cl abundances. Thus, pyrohydrolysis appears to incorporate fluid inclusion contributions, whereas SIMS analyses do not. Our calculations imply that FI host the majority (at least 80%) of Cl in Raspas eclogites; whether these fluid inclusions are all primary in nature, and therefore should be considered in the halogen budget of recycled eclogites, remains to be determined.

Combining SIMS and pyrohydrolysis techniques affords unique insights on the distribution and abundance of halogens in subducted slabs. SIMS provides detailed constraints on crystal lattice hosted halogen abundances and is well suited to determine bulk F concentrations, given the uncertainty that can be associated with pyrohydrolysis yields. Minimally retrogressed Raspas eclogites analyzed by SIMS contain between 145 and 258 µg/g F; F may be entirely hosted within the crystal lattice of eclogites, whereas only ~20% of Cl (at most), on average, is crystallographically hosted when FI are present. However, SIMS cannot accurately account for Cl abundances if primary fluid inclusions are present in the sample, which dominate the Cl budget of eclogites. Assuming that fluid inclusions observed here are primary features, pyrohydrolysis is the preferred method to measure the bulk Cl content of pristine FI-bearing rocks; minimally retrogressed Raspas eclogites analyzed by pyrohydrolysis contain between 6.7 and 11.3 µg/g Cl.

Implications

Previous studies have suggested that amphibole is the primary carrier of halogens to the upper mantle (Debret et al. 2016; Barnes et al. 2018). Our results suggest a more nuanced view when one

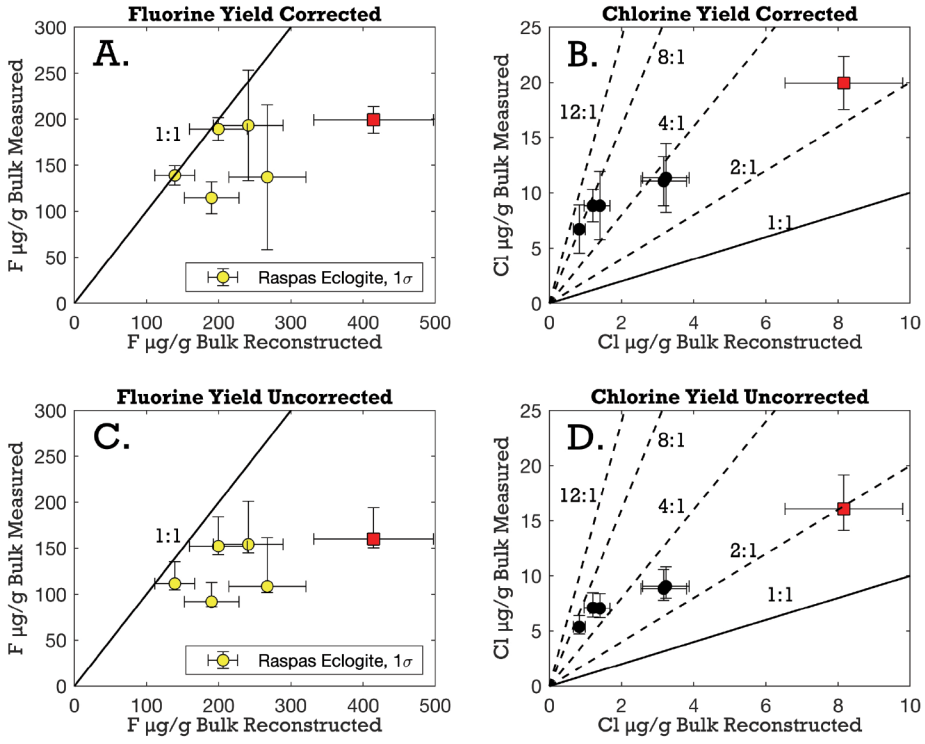

Figure 5. Bulk reconstructed and bulk measured (yield corrected) halogen abundances for F (**a**) and Cl (**b**). Y error bars show analytical reproducibility propagated with yield precision. Yield-uncorrected pyrohydrolysis values are shown in **c** and **d**, where positive Y error bars incorporate yield uncertainty. Red dots denote SEC46-02, which was not included in bulk calculations; see text for more information. Solid lines represent 1:1 lines; dashed lines plot various slopes, labeled accordingly. (Color online.)

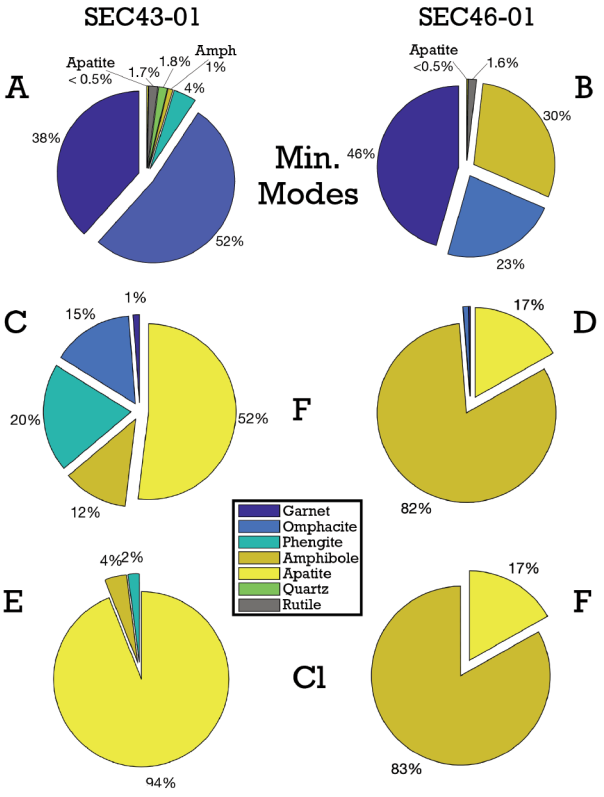

Figure 6. Pie diagrams show modal abundances (**a** and **b**), as well as the percent contribution from each phase to mineral-hosted halogen abundances as derived from SIMS analyses for F (**c** and **d**) and Cl (**e** and **f**) in two representative, yet mineralogically distinct, samples (Color online.).

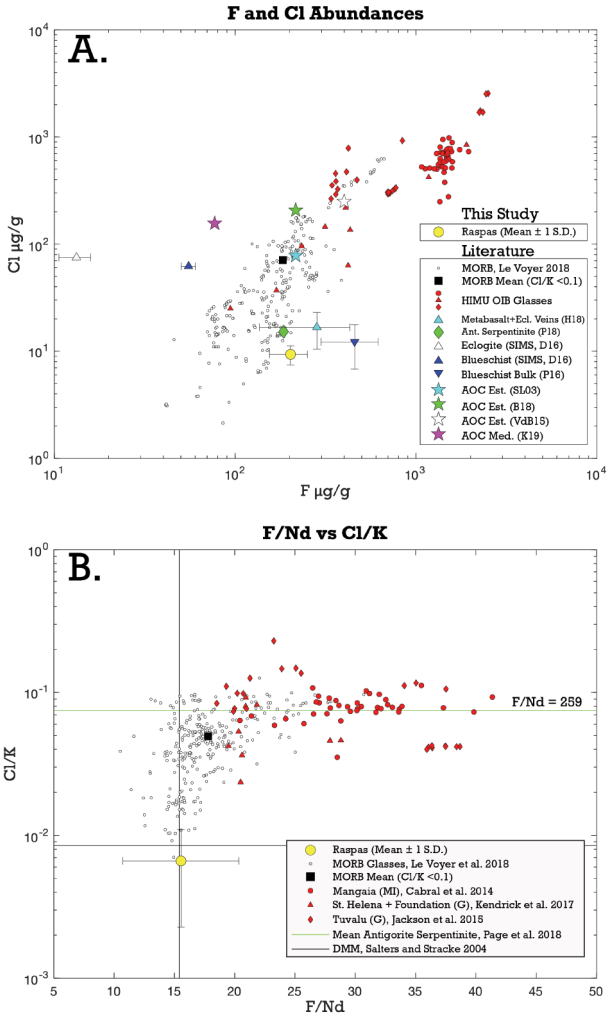

Figure 7. (**a**) F and Cl abundances from this study in comparison to literature values for MORB glasses from Le Voyer et al. (2018), HIMU OIB (Cabral et al. 2014; Jackson et al. 2015; Kendrick et al. 2017), blueschist and eclogite (Debret et al. 2016; Pagé et al. 2016; Hughes et al. 2018), antigorite serpentinite (Pagé et al. 2018), and AOC estimates (Straub and Layne 2003; Van den Bleeken and Koga 2015; Barnes et al. 2018; Kendrick 2019a). MORB with Cl/K values in excess of 0.1 were screened out, due to possible seawater contamination after Shimizu et al. (2016) and references therein. Peridotite mantle plots off the scale and would be 1.4–31 µg/g for F and from 0.14 to 0.38 µg/g for Cl (Urann et al. 2017). (**a**) F/Nd and Cl/K ratios of Raspas samples (Nd and K from John et al. 2010), MORB glasses from Le Voyer et al. (2018), mean antigorite serpentinite halogen concentrations from Pagé et al. (2018) with DMM K (60 µg/g) and Nd (0.713 µg/g) values of Salters and Stracke (2004), and OIB MIs and glasses from the literature (Cabral et al. 2014; Jackson et al. 2015; Kendrick et al. 2017). We note that our eclogitized AOC samples indeed plot below the canonical F/Nd of 21, as posited by Rose-Koga et al. (2012) for deeply subducted oceanic crust. (Color online.)

takes into account the contributions from coexisting phases and FI; amphibole's contribution to mineral-hosted bulk F and Cl abundances range from 6–84% and 4–85%, respectively (Fig. 6 and Supplemental[1] Fig. S7). When amphibole modes are below ~5% (three of six samples), apatite is the most important carrier for mineral-hosted halogens, containing >80% of mineral-hosted Cl and 38–71% of mineral-hosted F. Apatite is thought to be stable to 7.5 GPa at 950° (Konzett and Frost 2009), and will act as an important halogen carrier in eclogitized ocean crust. The remaining F is distributed between amphibole (4–53%), phengite (6–32%), omphacite (4–16%), and garnet (up to 2.2%). The above calculations consider only crystal matrix hosted halogen abundances; our results further indicate that FI host the majority of Cl in the bulk rock (at least 80%, on average). The ultimate fate of Cl will be dictated by the redistribution of free fluid phases during subsequent phase transformations, diffusive re-equilibration, and dynamic recrystallization at higher pressures and temperatures.

Raspas reconstructed bulk F concentrations (145–258 µg/g) are similar to previous pre-subduction altered oceanic crust (AOC) estimates of 216 µg/g (Straub and Layne 2003), blueschist (457 ± 159 µg/g F), and eclogite-facies (283 ± 146 µg/g F) AOC (Pagé et al. 2016; Hughes et al. 2018), as well as mean N-MORB values of 183 ± 107 µg/g calculated from recent work from Le Voyer et al. (2018) (Fig. 7a). Therefore, F concentrations remain relatively unchanged during the progression from nascent MORB, to AOC, and finally eclogitized AOC. Our results indicate that F is efficiently returned (~95%, derived from SIMS) to the upper mantle during subduction (Straub and Layne 2003; John et al. 2011; Pagé et al. 2016). Conversely, bulk pyrohydrolysis Cl measurements

(6.7–11.3 µg/g) are at least an order of magnitude lower than pre-subduction AOC estimates (e.g., 207 µg/g; Barnes and Cisneros 2012). Yet, observed Raspas concentrations are quite similar to recent blueschist and eclogite-facies AOC estimates by Hughes et al. (2018) of 3–23 µg/g Cl and Pagé et al. (2018) of 12 µg/g Cl, and well within the range observed in MORB (excluding Cl/K > 0.1 after Shimizu et al. 2016 and references therein) (Fig. 7a). Progression from initial MORB generation to seafloor alteration leads to an increase in Cl content, while subsequent eclogitization leads to a decrease in Cl abundances, returning to values similar to MORB. Using the pre-subduction AOC Cl bulk-rock estimate of Barnes and Cisneros (2012) of 207 µg/g Cl and data presented here, we calculate that the vast majority (>95%, derived from bulk pyrohydrolysis) of subducted Cl is expelled from the slab by the time the AOC parcel equilibrates at eclogite-facies conditions (Table 3), in agreement with previous workers (Straub and Layne 2003; John et al. 2011; Kendrick et al. 2014; Pagé et al. 2016). What little Cl remains will reside primarily in FI (at least 80%, on average). Thus, while most F is retained in the subducting slab at eclogite-facies conditions, most Cl previously added through hydrothermal alteration is expelled, fractionating F from Cl in eclogitized AOC. Yet, halogen abundances in Raspas are similar to unaltered MORB (Fig. 7a), while ratios of F and Cl with elements of similar compatibility during melting, Cl/K (0.0066 ± 0.0043), Cl/Nb (3.9 ± 1.0), and F/Nd (15.5 ± 4.8), are indistinguishable within uncertainty from depleted MORB mantle (DMM) ratios of Salters and Stracke (2004) (Fig. 7b).

The HIMU (high U/Pb) mantle source is thought to contain ancient altered oceanic crust based on Pb isotope systematics (and more recently Tl, see Shu et al. 2019), yielding enrichments in F/Nd, $^{35}Cl/^{37}Cl$, and often Cl/K and Cl/Nb ratios (Chase 1981; Hofmann and White 1982; Zindler et al. 1982; Stroncik and Haase 2004; John et al. 2011; Cabral et al. 2014; Jackson et al. 2015; Le Voyer et al. 2015; Kendrick et al. 2017; Rose-Koga et al. 2017; Hanyu et al. 2019). Our data indicate that halogen enrichments, and elevated F/Nd and Cl/K ratios, in the HIMU source cannot be produced by simple addition of recycled eclogitized AOC (Fig. 7b), but instead require delivery by an additional lithology, e.g., serpentinite as proposed by Kendrick et al. (2017), or an efficient fractionation mechanism to elevate halogen ratios during subsequent processing (e.g., Niu and O'Hara 2003). The broad spectrum of F/Nd and Cl/K ratios observed in HIMU melts may then reflect variable contributions from subducted serpentinite (green line, Fig. 7b). However, antigorite serpentinite breakdown by the reaction: antigorite = olivine + orthopyroxene + H_2O requires geochemical transfer of halogens, likely into a fluid phase as both F and Cl are highly incompatible in olivine and orthopyroxene (Dalou et al. 2014; Joachim et al. 2015; Beyer et al. 2016); their ultimate host within the upper mantle remains unknown. Direct phase transformation from antigorite serpentinite to the dense hydrous magnesium silicate Phase A may occur along cold geothermal gradients (Schmidt and Poli 1998), or halogens may become more compatible in K-rich clinopyroxene at increasing pressures as K solubility in clinopyroxene increases to ~1 wt% K_2O at 100 kbar (Schmidt and Poli 1998). Thus, subduction proceeds in returning to the upper mantle an eclogitized AOC parcel with halogen ratios quite similar to the MORB from which it was derived.

Acknowledgments and Funding

We thank two anonymous reviewers for their insights and suggestions, which improved the manuscript. This research was supported by NSF award EAR-P&G no. 1524311 and no. 1839128 to VLR. B.M.U. acknowledges the support of the WHOI Ocean Venture Fund. This work was also supported by NSF-PIRE grant (OIA-1545903) to J.D.B.

References cited

Anderson, A.T., and Greenland, L.P. (1969) Phosphorus fractionation diagram as a quantitative indicator of crystallization differentiation of basaltic liquids. Geochimica et Cosmochimica Acta, 33, 493–505.

Armstrong, J.T. (1995) CITZAF—a package of correction programs for the quantitative electron microbeam X-ray analysis of thick polished materials, thin films, and particles. Microbeam Analysis, 177–200.

Barnes, J.D., and Cisneros, M. (2012) Mineralogical control on the chlorine isotope composition of altered oceanic crust. Chemical Geology, 326-327, 51–60.

Barnes, J.D., Manning, C.E., Scambelluri, M., and Selverstone, J. (2018) The Behavior of Halogens During Subduction-Zone Processes. In D.E. Harlov, Ed., The Role of Halogens in Terrestrial and Extraterrestrial Geochemical Processes, 263, pp. 545–590. Springer.

Beinlich, A., Klemd, R., John, T., and Gao, J. (2010) Trace-element mobilization during Ca-metasomatism along a major fluid conduit: Eclogitization of blueschist as a consequence of fluid–rock interaction. Geochimica et Cosmochimica Acta, 74, 1892–1922.

Beyer, C., Klemme, S., Grützner, T., Ireland, T.R., Magee, C.W., and Frost, D.J. (2016) Fluorine partitioning between eclogitic garnet, clinopyroxene, and melt at upper mantle conditions. Chemical Geology, 437, 88–97.

Cabral, R.A., Jackson, M.G., Koga, K.T., Rose-Koga, E.F., Hauri, E.H., Whitehouse, M.J., Price, A.A., Day, J.M.D., Shimizu, N., and Kelley, K.A. (2014) Volatile cycling of H_2O, CO_2, F, and Cl in the HIMU mantle: A new window provided by melt inclusions from oceanic hot spot lavas at Mangaia, Cook Islands. Geochemistry, Geophysics, Geosystems, 15, 4445–4467.

Chase, C.G. (1981) Oceanic island Pb: Two-stage histories and mantle evolution. Earth and Planetary Science Letters, 52, 277–284.

Chavrit, D., Burgess, R., Sumino, H., Teagle, D.A.H., Droop, G., Shimizu, A., and Ballentine, C.J. (2016) The contribution of hydrothermally altered ocean crust to the mantle halogen and noble gas cycles. Geochimica et Cosmochimica Acta, 183, 106–124.

Dalou, C., Koga, K.T., Le Voyer, M., and Shimizu, N. (2014) Contrasting partition behavior of F and Cl during hydrous mantle melting: implications for Cl/F signature in arc magmas. Progress in Earth and Planetary Science, 1, 26.

Debret, B., Koga, K.T., Cattani, F., Nicollet, C., Van den Bleeken, G., and Schwartz, S. (2016) Volatile (Li, B, F and Cl) mobility during amphibole breakdown in subduction zones. Lithos, 244, 165–181.

Feininger, T. (1980) Eclogite and related high-pressure regional metamorphic rocks from the Andes of Ecuador. Journal of Petrology, 21, 107–140.

——— (1987) Allochthonous terranes in the Andes of Ecuador and northwestern Peru. Canadian Journal of Earth Sciences, 24, 266–278.

Freundt, A., Grevemeyer, I., Rabbel, W., Hansteen, T.H., Hensen, C., Wehrmann, H., Kutterolf, S., Halama, R., and Frische, M. (2014) Volatile (H_2O, CO_2, Cl, S) budget of the Central American subduction zone. International Journal of Earth Sciences, 103, 2101–2127.

Gabriele, P. (2002) HP terranes exhumation in an active margin setting: geology, petrology and geochemistry of the Raspas Complex in SW Ecuador. Ph.D. thesis, University of Lausanne, Switzerland.

Gale, A., Dalton, C.A., Langmuir, C.H., Su, Y., and Schilling, J.G. (2013) The mean composition of ocean ridge basalts. Geochemistry, Geophysics, Geosystems, 14, 489–518.

Gao, J., and Klemd, R. (2001) Primary fluids entrapped at blueschist to eclogite transition: evidence from the Tianshan meta-subduction complex in northwestern China. Contributions to Mineralogy and Petrology, 142, 1–14.

Halama, R., John, T., Herms, P., Hauff, F., and Schenk, V. (2011) A stable (Li, O) and radiogenic (Sr, Nd) isotope perspective on metasomatic processes in a subducting slab. Chemical Geology, 281, 151–166.

Hanyu, T., Shimizu, K., Ushikubo, T., Kimura, J.-I., Chang, Q., Hamada, M., Ito, M., Iwamori, H., and Ishikawa, T. (2019) Tiny droplets of ocean island basalts unveil Earth's deep chlorine cycle. Nature Communications, 10, 222.

Herms, P., John, T., Bakker, R.J., and Schenk, V. (2012) Evidence for channelized external fluid flow and element transfer in subducting slabs (Raspas Complex, Ecuador). Chemical Geology, 310-311, 79–96.

Hofmann, A.W., and White, W.M. (1982) Mantle plumes from ancient oceanic crust. Earth and Planetary Science Letters, 57, 421–436.

Hughes, L., Burgess, R., Chavrit, D., Pawley, A., Tartèse, R., Droop, G., Ballentine, C.J., and Lyon, I. (2018) Halogen behaviour in subduction zones: Eclogite facies rocks from the Western and Central Alps. Geochimica et Cosmochimica Acta, 243, 1–23.

Imai, N., Terashima, S., Itoh, S., and Ando, A. (1995) 1994 Complilation of Analyitical Data for Minor and Trace Elements in Seventeen GSJ Geochemical Reference Samples, "Igneous Rock Series." Geostandards and Geoanalytical Research, 19, 135–213.

Ito, E., Harris, D.M., and Anderson, A.T. (1983) Alteration of oceanic crust and geologic cycling of chlorine and water. Geochimica et Cosmochimica Acta, 47, 1613–1624.
Jackson, M.G., Koga, K.T., Price, A., Konter, J.G., Koppers, A.A.P., Finlayson, V.A., Konrad, K., Hauri, E.H., Kylander-Clark, A., Kelley, K.A., and Kendrick, M.A. (2015) Deeply dredged submarine HIMU glasses from the Tuvalu Islands, Polynesia: implications for volatile budgets of recycled oceanic crust. Geochemistry, Geophysics, Geosystems, 16, 3210–3234.
Joachim, B., Pawley, A., Lyon, I.C., Marquardt, K., Henkel, T., Clay, P.L., Ruzié, L., Burgess, R., and Ballentine, C.J. (2015) Experimental partitioning of F and Cl between olivine, orthopyroxene and silicate melt at Earth's mantle conditions. Chemical Geology, 416, 65–78.
John, T., and Schenk, V. (2003) Partial eclogitisation of gabbroic rocks in a late Precambrian subduction zone (Zambia): prograde metamorphism triggered by fluid infiltration. Contributions to Mineralogy and Petrology, 146, 174–191.
John, T., Scambelluri, M., Frische, M., Barnes, J.D., and Bach, W. (2011) Dehydration of subducting serpentinite: Implications for halogen mobility in subduction zones and the deep halogen cycle. Earth and Planetary Science Letters, 308, 65–76.
John, T., Scherer, E.E., Schenk, V., Herms, P., Halama, R., and Garbe-Schönberg, D. (2010) Subducted seamounts in an eclogite-facies ophiolite sequence: the Andean Raspas Complex, SW Ecuador. Contributions to Mineralogy and Petrology, 159, 265–284.
Kendrick, M.A. (2018) Halogens in seawater, marine sediments and the altered oceanic lithosphere. In D.E. Harlov, Ed., The Role of Halogens in Terrestrial and Extraterrestrial Geochemical Processes, 87, pp. 591–648. Springer.
——— (2019a) Halogens in altered ocean crust from the East Pacific Rise (ODP/IODP Hole 1256D). Geochimica et Cosmochimica Acta, 261, 93–112.
——— (2019b) Halogens in Atlantis Bank gabbros, SW Indian Ridge: Implications for styles of seafloor alteration. Earth and Planetary Science Letters, 514, 96–107.
Kendrick, M.A., Jackson, M.G., Kent, A.J.R., Hauri, E.H., Wallace, P.J., and Woodhead, J. (2014) Contrasting behaviours of CO_2, S, H_2O and halogens (F, Cl, Br, and I) in enriched-mantle melts from Pitcairn and Society seamounts. Chemical Geology, 370, 69–81.
Kendrick, M.A., Honda, M., and Vanko, D.A. (2015) Halogens and noble gases in Mathematician Ridge meta-gabbros, NE Pacific: implications for oceanic hydrothermal root zones and global volatile cycles. Contributions to Mineralogy and Petrology, 170, 173.
Kendrick, M.A., Hémond, C., Kamenetsky, V.S., Danyushevsky, L., Devey, C.W., Rodemann, T., Jackson, M.G., and Perfit, M.R. (2017) Seawater cycled throughout Earth's mantle in partially serpentinized lithosphere. Nature Geoscience, 10, 222–228.
Konzett, J., and Frost, D.J. (2009) The high P–T stability of hydroxyl-apatite in natural and simplified MORB—an experimental study to 15 GPa with implications for transport and storage of phosphorus and halogens in subduction zones. Journal of Petrology, 50, 2043–2062.
Kumamoto, K.M., Warren, J.M., and Hauri, E.H. (2017) New SIMS reference materials for measuring water in upper mantle minerals. American Mineralogist, 102, 537–547.
Kusebauch, C., John, T., Whitehouse, M.J., and Engvik, A.K. (2015) Apatite as probe for the halogen composition of metamorphic fluids (Bamble Sector, SE Norway). Contributions to Mineralogy and Petrology, 170, 271.
Le Voyer, M., Cottrell, E., Kelley, K.A., Brounce, M., and Hauri, E.H. (2015) The effect of primary versus secondary processes on the volatile content of MORB glasses: An example from the equatorial Mid-Atlantic Ridge (5°N–3°S). Journal of Geophysical Research: Solid Earth, 120, 125–144.
Le Voyer, M., Hauri, E.H., Cottrell, E., Kelley, K.A., Salters, V.J.M., Langmuir, C.H., Hilton, D.R., Barry, P.H., and Füri, E. (2019) Carbon fluxes and primary magma CO_2 contents along the global mid-ocean ridge system. Geochemistry, Geophysics, Geosystems, 20(3), 1387–1424.
Locock, A.J. (2014) An Excel spreadsheet to classify chemical analyses of amphiboles following the IMA 2012 recommendations. Computers & Geosciences, 62, 1–11.
Marschall, H.R., Altherr, R., Gméling, K., and Kasztovszky, Z. (2009) Lithium, boron and chlorine as tracers for metasomatism in high-pressure metamorphic rocks: a case study from Syros (Greece). Mineralogy and Petrology, 95, 291–302.
Maruyama, S., Liou, J.G., and Terabayashi, M. (1996) Blueschists and eclogites of the world and their exhumation. International Geology Review, 38, 485–594.
Massonne, H.J. (2012) Formation of amphibole and clinozoisite–epidote in eclogite owing to fluid infiltration during exhumation in a subduction channel. Journal of Petrology, 53, 1969–1998.
Massonne, H.J., and Schreyer, W. (1987) Phengite geobarometry based on the limiting assemblage with K-feldspar, phlogopite, and quartz. Contributions to Mineralogy and Petrology, 96, 212–224.
Mather, T.A., Pyle, D.M., Tsanev, V.I., McGonigle, A.J.S., Oppenheimer, C., and Allen, A.G. (2006) A reassessment of current volcanic emissions from the Central American arc with specific examples from Nicaragua. Journal of Volcanology, 149, 297–311.
Niu, Y., and O'Hara, M.J. (2003) Origin of ocean island basalts: A new perspective from petrology, geochemistry, and mineral physics considerations. Journal of Geophysical Research: Solid Earth, 108, 63.
Pagé, L., Hattori, K., and Guillot, S. (2018) Mantle wedge serpentinites: A transient reservoir of halogens, boron, and nitrogen for the deeper mantle. Geology, 46, 883–886.
Pagé, L., Hattori, K., de Hoog, J.C.M., and Okay, A.I. (2016) Halogen (F, Cl, Br, I) behaviour in subducting slabs: A study of lawsonite blueschists in western Turkey. Earth and Planetary Science Letters, 442, 133–142.
Philippot, P., and Selverstone, J. (1991) Trace-element-rich brines in eclogitic veins: implications for fluid composition and transport during subduction. Contributions to Mineralogy and Petrology, 106, 417–430.
Philippot, P., Agrinier, P., and Scambelluri, M. (1998) Chlorine cycling during subduction of altered oceanic crust. Earth and Planetary Science Letters, 161, 33–44.
Pyle, D.M., and Mather, T.A. (2009) Halogens in igneous processes and their fluxes to the atmosphere and oceans from volcanic activity: A review. Chemical Geology, 263, 110–121.
Rebay, G., Powell, R., and Diener, J.F.A. (2010) Calculated phase equilibria for a morb composition in a P-T range, 450–650 °C and 18–28 kbar: the stability of eclogite. Journal of Metamorphic Geology, 28, 635–645.
Rose-Koga, E.F., Koga, K.T., Schiano, P., Le Voyer, M., Shimizu, N., Whitehouse, M.J., and Clocchiatti, R. (2012) Mantle source heterogeneity for South Tyrrhenian magmas revealed by Pb isotopes and halogen contents of olivine-hosted melt inclusions. Chemical Geology, 334, 266–279.
Rose-Koga, E.F., Koga, K.T., Moreira, M., Vlastelic, I., Jackson, M.G., Whitehouse, M.J., Shimizu, N., and Habib, N. (2017) Geochemical systematics of Pb isotopes, fluorine, and sulfur in melt inclusions from São Miguel, Azores. Chemical Geology, 458, 22–37.
Sadofsky, S.J., Portnyagin, M., Hoernle, K., and van den Bogaard, P. (2008) Subduction cycling of volatiles and trace elements through the Central American volcanic arc: evidence from melt inclusions. Contributions to Mineralogy and Petrology, 155, 433–456.
Salters, V.J.M., and Stracke, A. (2004) Composition of the depleted mantle. Geochemistry, Geophysics, Geosystems, 5.
Scambelluri, M., and Philippot, P. (2001) Deep fluids in subduction zones. Lithos, 55, 213–227.
Schmidt, M.W., and Poli, S. (1998) Experimentally based water budgets for dehydrating slabs and consequences for arc magma generation. Earth and Planetary Science Letters, 163, 361–379.
Schnetger, B., and Muramatsu, Y. (1996) Determination of halogens, with special reference to iodine, in geological and biological samples using pyrohydrolysis for preparation and inductively coupled plasma mass spectrometry and ion chromatography for measurement. The Analyst, 121, 1627.
Shimizu, K., Saal, A.E., Myers, C.E., Nagle, A.N., Hauri, E.H., Forsyth, D.W., Kamenetsky, V.S., and Niu, Y. (2016) Two-component mantle melting-mixing model for the generation of mid-ocean ridge basalts: Implications for the volatile content of the Pacific upper mantle. Geochimica et Cosmochimica Acta, 176, 44–80.
Shu, Y., Nielsen, S.G., Marschall, H.R., John, T., Blusztajn, J., and Auro, M. (2019) Closing the loop: Subducted eclogites match thallium isotope compositions of ocean island basalts. Geochimica et Cosmochimica Acta, 250, 130–148.
Stormer, J.C., and Pierson, M. (1993) Variation of F and Cl X-ray intensity due to anisotropic diffusion in apatite during electron microprobe analysis. American Mineralogist, 78, 641–648.
Straub, S.M., and Layne, G.D. (2003) The systematics of chlorine, fluorine, and water in Izu arc front volcanic rocks: Implications for volatile recycling in subduction zones. Geochimica et Cosmochimica Acta, 67, 4179–4203.
Stroncik, N.A., and Haase, K.M. (2004) Chlorine in oceanic intraplate basalts: Constraints on mantle sources and recycling processes. Geology, 32, 945.
Svensen, H., Jamtveit, B., Banks, D.A., and Austrheim, H. (2001) Halogen contents of eclogite facies fluid inclusions and minerals: Caledonides, western Norway. Journal of Metamorphic Geology, 19, 165–178.
Turcotte, D.L., and Schubert, G. (2002) Geodynamics by Donald L. Turcotte, 2nd ed. Cambridge University Press.
Urann, B.M., Le Roux, V., Hammond, K., Marschall, H.R., Lee, C.T.A., and Monteleone, B.D. (2017) Fluorine and chlorine in mantle minerals and the halogen budget of the Earth's mantle. Contributions to Mineralogy and Petrology, 172, 324.
Van den Bleeken, G., and Koga, K.T. (2015) Experimentally determined distribution of fluorine and chlorine upon hydrous slab melting, and implications for F–Cl cycling through subduction zones. Geochimica et Cosmochimica Acta, 171, 353–373.
Watson, E. (1979) Apatite saturation in basic to intermediate magmas. Geophysical Research Letters, 6(12), 937–940.
Zack, T., Rivers, T., and Foley, S. (2001) Cs–Rb–Ba systematics in phengite and amphibole: an assessment of fluid mobility at 2.0 GPa in eclogites from Trescolmen, Central Alps. Contributions to Mineralogy and Petrology, 140, 651–669.
Zindler, A., Jagoutz, E., and Goldstein, S. (1982) Nd, Sr and Pb isotopic systematics in a three-component mantle: a new perspective. Nature, 298, 519–523.

Manuscript received February 7, 2019
Manuscript accepted November 10, 2019
Manuscript handled by Anita Cadoux

Endnote:

[1]Deposit item AM-20-36994, Supplemental Figures and Tables. Deposit items are free to all readers and found on the MSA website, via the specific issue's Table of Contents (go to http://www.minsocam.org/MSA/AmMin/TOC/2020/Mar2020_data/Mar2020_data.html).